Water Science & Technology

Water Science & Technology Vol 84 No 9, 2541 doi: 10.2166/wst.2021.364

Fabricating novel PVDF-g-IBMA copolymer hydrophilic ultrafiltration membrane for treating papermaking wastewater with good antifouling property

Yujia Tong, Wenlong Ding, Lijian Shi and Weixing Li*

State Key Laboratory of Materials-Oriented Chemical Engineering, College of Chemical Engineering, Nanjing Tech University, Nanjing 210009, China
*Corresponding author. E-mail: wxli@njtech.edu.cn

ABSTRACT

Ultrafiltration membranes are widely used for the treatment of papermaking wastewater. The antifouling performance of polyvinylidene fluoride (PVDF) ultrafiltration membranes can be improved by changing the hydrophilicity. Here, a novel amphiphilic copolymer material, PVDF grafted with N-isobutoxy methacrylamide (PVDF-g-IBMA), was prepared using ultraviolet-induced Cu(II)-mediated reversible deactivation radical polymerization. The amphipathic copolymer was used to prepare ultrafiltration membrane via NIPS. The prepared PVDF-g-IBMA ultrafiltration membrane was estimated using ^{1}H NMR, FT-IR, and DSC. The contact angle, casting viscosity, and the permeation performance of the PVDF-g-IBMA ultrafiltration membrane were also determined. The pure water flux, bovine serum albumin removal rate, and pure water flux recovery rate of the PVDF-g-IBMA ultrafiltration membrane were 432.8 L·m^{-2}·h^{-1}, 88.4%, and 90.8%, respectively. Furthermore, for the treatment of actual papermaking wastewater, the chemical oxygen demand and turbidity removal rates of the membrane were 61.5% and 92.8%, respectively. The PVDF-g-IBMA amphiphilic copolymer ultrafiltration membrane exhibited good hydrophilicity and antifouling properties, indicating its potential for treating papermaking wastewater.

Key words: antifouling, papermaking wastewater, ultrafiltration membrane, UV-induced Cu(II)-mediated RDRP

HIGHLIGHTS

- A novel amphiphilic copolymer PVDF-g-IBMA prepared by UV-induced RDRP.
- Good hydrophilic and anti-fouling properties of PVDF-g-IBMA copolymer UF membrane.
- The MWCO, BSA rejection rate and pure water recovery ratio were 43.7 kDa, 88.4% and 90.8%, respectively.
- For treating actual papermaking wastewater, the COD removal rate reached 61.5%.

NOMENCLATURE

J	Membrane permeation flux, L·m^{-2}·h^{-1}
V	Volume of pure water permeated through the membrane, L
A	Effective surface area of the membrane, m^2
Δt	Permeation time, h
R	BSA rejection rate, %
C_p	Protein concentrations in the permeate, g·L^{-1}
C_f	Protein concentrations in the feed, g·L^{-1}
FRR	Pure water recovery ratio, %
J_r	Original pure water flux, L·m^{-2}·h^{-1}
J_w	Recovered water flux, L·m^{-2}·h^{-1}
COD	Chemical oxygen demand, mg·L^{-1}

1. INTRODUCTION

Water shortage is a major crisis affecting human health and sustainable economic and social development. Ultrafiltration membrane (UF) technology is used for the treatment of papermaking wastewater to comprehensively remove impurities from wastewater (Gönder *et al.* 2012; Toczyłowska-Mamińska 2017; Haq *et al.* 2020). Particularly, high-performance UF

membranes are important for water purification. The materials used for preparing UF membranes determine the efficiency of separation technology (Shen *et al.* 2020; Sun *et al.* 2020; Zhang *et al.* 2020). Commercial polyvinylidene fluoride (PVDF) membranes exhibit a low surface energy and high hydrophobicity, which facilitates the adsorption of proteins or organics on the pores and surface of membranes (Gao *et al.* 2011; Gao *et al.* 2019; Chen *et al.* 2021). Then, the significantly low permeation flux of fouling PVDF membranes owing to their high filtration resistance has restricted their further application . In addition, the issues associated with cleaning PVDF membranes affect their application cost and reduce their service life (Sri Abirami Saraswathi *et al.* 2018; Sierke & Ellis 2019). Thus, it is important to improve the hydrophilic properties of PVDF UF membranes to extend their application.

PVDF membranes containing materials with hydrophilic groups exhibit a higher water transfer rate and lower filtration resistance than pure PVDF membranes, indicating their potential as high-performance separation membranes (Liu *et al.* 2011; Park *et al.* 2018; Matyjaszewski 2020). Amphiphilic polymers are branched macromolecules with branching periodicity and structural symmetry (Zhang & Dai 2019). These monodisperse branched macromolecules have numerous terminal groups on their surfaces, which increase their surface functionality and reactivity. During the phase inversion of membranes prepared using the homopolymer obtained by grafting an amphiphilic copolymer with PVDF, the hydrophilic chains of the amphiphilic copolymer migrate to the membrane surface, thus minimizing the interface free energy of the membrane. This is because the hydrophobic chains of amphiphilic copolymers are compatible with the main body of PVDF, whereas the hydrophilic chains achieve hydrophilicity through self-assembly and surface migration. Zhao *et al.* (2019) prepared polyacryloylmorpholine-b-poly(methyl methacrylate)-b-polyacryloylmorpholine (PAMA) using the reversible addition–fragmentation chain transfer polymerization method to fabricate a PVDF/PAMA UF membrane. The water flux, bovine serum albumin (BSA) retention, and recovery rate of the PVDF/PAMA membrane were 236 $L{\cdot}m^{-2}{\cdot}h^{-1}$, 98.3%, and 98.1%, respectively. Minehara *et al.* (2014) blended PVDF, methyl methacrylate, and polyethylene glycol methyl methacrylate copolymer (PMMA-g-PEO) to prepare a PVDF/PMMA-g-PEO membrane using the non-solvent induced phase separation (NIPS) method. The flux and rejection rate of polystyrene latex with a PVDF/PMMA-g-PEO membrane diameter of 88 nm were 29–50 $L{\cdot}m^{-2}{\cdot}h^{-1}$ and >96%, respectively. Wu *et al.* (2019) blended PVDF-grafted poly(ethylene glycol) methyl ether methacrylate (PEGMA) to prepare a PVDF/PVDF-g-PEGMA membrane. The flux, alginate rejection rate, and water flux recovery rate of the membrane were 700 $L{\cdot}m^{-2}{\cdot}h^{-1}$, 87%–100%, respectively, indicating the good antifouling of the membrane. These findings indicate that amphiphilic polymers can be used to improve the hydrophilic properties of PVDF UF membranes.

Ultraviolet (UV)-induced Cu(II)-mediated reversible deactivation radical polymerization (RDRP) is an environmentally friendly synthesis technology which combines UV stimulation and Cu(II)-mediated RDRP (Chuang *et al.* 2014; Hu *et al.* 2018a, 2018b). UV-induced Cu(II)-mediated RDRP can be used to modify pure PVDF membranes as it enables a more compact combination of hydrophobic and hydrophilic chains to ensure that the hydrophilic chain is fixed on the surface of the PVDF membranes (Cui *et al.* 2019; Zou *et al.* 2020; Li *et al.* 2021). Therefore, the addition of amphiphilic copolymers to PVDF membranes can improve the hydrophilicity and antifouling properties. In addition, the self-assembly capability of amphiphilic copolymers endows pure PVDF membranes with a higher permeation flux and narrow membrane pore size distribution (Guillen *et al.* 2011). Lei *et al.* (2018) used PVDF and tetrahydrofurfuryl methacrylate as raw materials to develop a new amphiphilic polymer membrane (THFMA, PVDF-g-THFMA) through photoinduced Cu(II)-mediated RDRP. The water flux and BSA rejection rate of the PVDF-g-THFMA copolymer UF membrane were 293.9 $L{\cdot}m^{-2}{\cdot}h^{-1}$ and 91.3%, respectively. Tong *et al.* (2020) prepare a novel amphiphilic copolymer of PVDF grafted with 1-Methyl-2-pyrrolidone (NMA, PVDF-g-NMA) using the same method. The water flux and BSA rejection rate of the PVDF-g-NMA copolymer UF membrane were 272.1 $L{\cdot}m^{-2}{\cdot}h^{-1}$ and 92.6%, respectively.

Papermaking wastewater has a complex composition and contains a large amount of lignin, hemicellulose, sugars, and other dissolved substances with high suspended solids, turbidity, and chemical oxygen demand (COD), which affect the survival of aquatic organisms. Generally, papermaking wastewater is treated using a combination of physical (e.g., PVDF UF using the membrane), chemical, and biological methods. The Ministry of Environmental Protection has recently stipulated that COD emissions are 80–100 mg/L, and the special emission limit is less than 50 mg/L. The papermaking enterprises are required to increase their efforts in the treatment of papermaking wastewater. Although previous studies have successfully improved the hydrophilicity of PVDF UF membranes, these membranes have not been applied in actual wastewater systems. N-Isobutoxy methacrylamide (IBMA) is a new energy-saving and environmentally friendly crosslinking monomer that can be used to improve the adhesion of polar substrates under UV radiation. In this work, we propose to prepare PVDF-g-IBMA

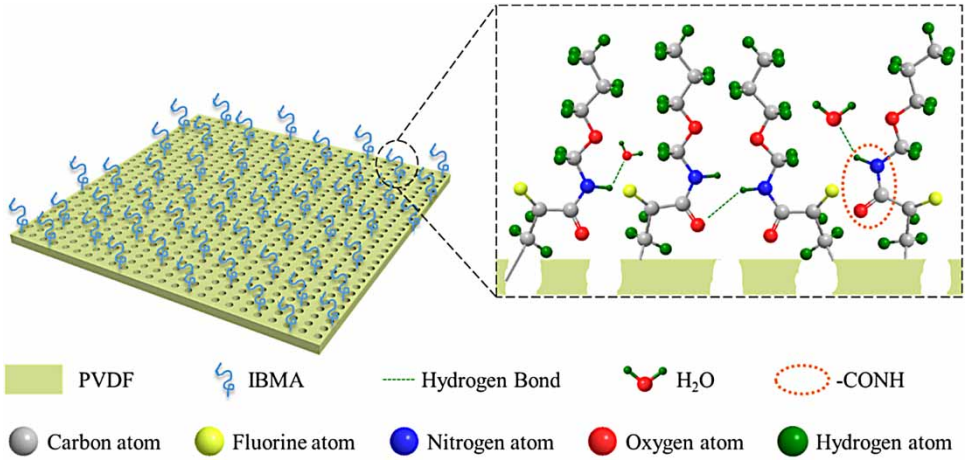

Figure 1 | The structure illustration of the PVDF-g-IBMA copolymer UF membrane.

copolymer by UV-induced Cu(II)-mediated RDRP using IBMA as a monomer as showed in Figure 1. We suppose the novel developed PVDF-g-IBMA membrane exhibits better hydrophilicity and antifouling properties than PVDF UF membranes, indicating its prospect for the treatment of papermaking wastewater.

2. EXPERIMENTAL SECTION

2.1. Chemicals

PVDF (Solef105, Mw 5,700,000–600,000) was obtained from Solvay Specialty Polymers (Shanghai, China). IBMA THFMA, dextran (Mw 10,000, 40,000, 70,000, and 500,000 Da), Me6-Tre, and BSA (Mw 67,000 Da) were bought from Sigma-Aldrich (Shanghai, China). $CuCl_2$, KCl, NaCl, $Na_2HPO_4{\cdot}12H_2O$, and KH_2PO_4, and NMP was procured from Aladdin Industrial Corporation (Shanghai, China).

2.2. Preparation of the PVDF-g-IBMA ultrafiltration membrane

PVDF (1.5 g), NMP (10 mL), and $CuCl_2$ (0.02 g) were added to a quartz reactor equipped with a rotor. The solution was purged with argon under stirring for 1 h to remove dissolved oxygen, after which Me6-Tren (0.1 mL) and IBMA solution (4.5 mL) were added to the solution (Figure 2). The obtained solution was polymerized by placing the solution in a UV reactor supplying 365 nm irradiation and protected under an argon atmosphere for 6 h. Subsequently, the obtained precipitate was washed with DI water three times to remove unreacted monomers. The obtained PVDF-g-IBMA was kept in an oven at 60 °C for further use.

PVDF-g-IBMA copolymer UF membranes were prepared using the NIPS method. The dried PVDF-g-IBMA copolymer was dissolved in a certain proportion of NMP solution in the three-necked flask (Table 1). The resulting casting solution was stirred in a 60 °C water bath with a mechanical stirrer with a speed of 0.2 kr/min for 4 h. The method of preparing the membrane

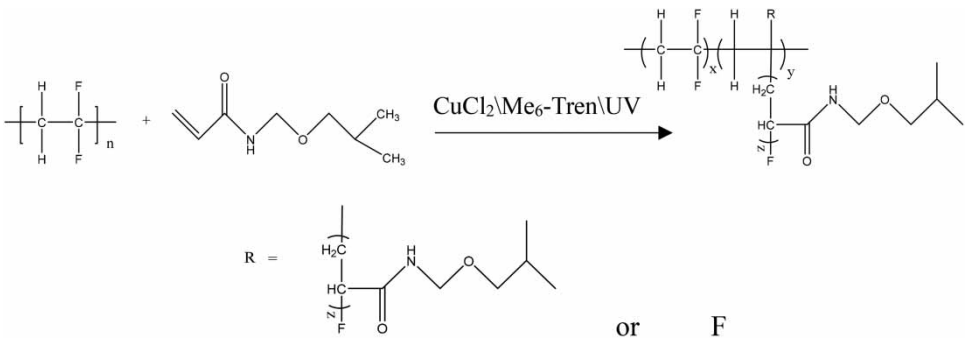

Figure 2 | Schematic diagram of grafting procedure between PVDF and IBMA.

Table 1 | Membrane prepared with different ratios

Membrane	PVDF (wt.%)	PVDF-g-IBMA (wt.%)	NMP (wt.%)
P15	15	/	85
P20	20	/	80
P25	25	/	75
I15	/	15	85
I20	/	20	80
I25	/	25	75

is the same as previously reported. The viscosity of the UF membrane casting solution was tested by selecting a suitable rotor and rotation speed.

2.3. Characterization of PVDF-g-IBMA copolymer UF membrane

The grafting reaction of the PVDF-g-IBMA copolymer was investigated using ^{1}H nuclear magnetic resonance (NMR, AVANCE AV-300, Bruker, Switzerland) spectroscopy. ^{1}H NMR spectroscopy sample was prepared by dissolving the PVDF-g-IBMA copolymer in deuterated dimethyl sulfoxide. The mass and molar fractions of IBMA in the PVDF-g-IBMA copolymer were calculated using Equations (1) and (2), respectively.

$$\varphi_w(IBMA) = \frac{\varphi_{m(IBMA)} \cdot M_{IBMA}}{\varphi_{m(IBMA)} \cdot M_{IBMA} + (1 - \varphi_{m(IBMA)}) \cdot M_{PVDF(unit)}} \tag{1}$$

$$\varphi_m(IBMA) = \frac{\frac{1}{15}(\mathrm{I}_a + \mathrm{I}_b + \mathrm{I}_c + \mathrm{I}_d + \mathrm{I}_e + \mathrm{I}_f)}{\frac{1}{15}(\mathrm{I}_a + \mathrm{I}_b + \mathrm{I}_c + \mathrm{I}_d + \mathrm{I}_e + \mathrm{I}_f) + \frac{1}{2}(\mathrm{I}_{a(hh)} + \mathrm{I}_{a(ht)})}, \tag{2}$$

where $\varphi_w(IBMA)$ and $\varphi_m(IBMA)$ are the mass and mole fractions of IBMA in PVDF-g-IBMA, respectively; I_X is the area of the corresponding peak in the ^{1}H NMR spectrum; and M_{IBMA} and $M_{PVDF(unit)}$ are the molecular weights of IBMA and PVDF, respectively.

The Fourier-transform infrared Spectrometer (FTIR) of the UF membranes were analyzed using a FTIR spectrometer (Cary660, Agilent, Australia) by attenuated total reflectance in the wavelength range of 4,000–500 cm^{-1}. The melting points of the PVDF and PVDF-g-IBMA copolymers were measured using differential scanning calorimetry (DSC, STA449F3, NETZSCH, Germany). SEM images of all the PVDF-g-IBMA UF membranes were attained using a scanning electron microscopy (SEM, Hitachi S4800, Japan) instrument. To examine the chemical compositions of copolymer membranes, the distributions of oxygen, carbon, and fluorine in the membrane were recorded using SEM equipped with an energy-dispersive X-ray spectrometer. The dynamic contact angles (DWCA) of the UF membranes were analyzed using a contact angle measuring instrument (DSA 100, Kruss, Germany). The WCAs were tested by placing a 3.0 μL DI water droplet on the membrane surfaces.

2.4. Separation performance

The pure water fluxes of the PVDF homopolymer and PVDF-g-IBMA copolymer UF membranes with an effective area (4.1 cm^2) were measured using an UF apparatus (Amicon 8400). For the analysis, first, the membranes were pre-compacted at 0.15 MPa for 20 min. Subsequently, the pure water fluxes of the UF membranes were recorded at 0.1 MPa for 5 min. The pure water fluxes of the UF membranes were calculated using Equation (3).

$$J = \frac{V}{A\ \Delta t} \tag{3}$$

where V is the volume of pure water permeated through the membrane (L), A is the effective surface area of the membrane (m^2), and Δt is the permeation time (h).

To determine the retention performance of the modified membrane, dextran solution was used as the filter medium by the method reported previously (Tong *et al.* 2020). Molecular weight cutoff (MWCO) is the membrane's retention rate of 90% for

dextran solution. Gel chromatography is used to analyze the molecular weight distribution of the solution on the feed side and the permeate side.

The antifouling performance of the PVDF homopolymer and PVDF-g-IBMA copolymer membranes was measured using the apparatus at 0.1 MPa for 60 min (Tong *et al.* 2020). The protein fouling potential of the PVDF-g-IBMA UF membranes was evaluated using a BSA solution. To prepare the BSA solution, first, PBS solution (pH 7.4) was prepared by adding NaCl (8.0 g), $Na_2HPO_4{\cdot}12H_2O$ (3.63 g), KCl (0.2 g), and KH_2PO_4 (0.24 g) to DI water (1.0 L). Subsequently, BSA (0.5 g) was mixed with the above solution to a concentration of 0.5 g/L.

The BSA rejection rate (R) of the prepared UF membranes was calculated using Equation (4).

$$R(\%) = \left(1 - \frac{C_p}{C_f}\right) \times 100\%, \tag{4}$$

where R is the BSA rejection rate, and C_p and C_f are the protein concentrations in the permeate and feed (g/L), respectively. The C_p and C_f values were resolved using a Ultraviolet-visible Spectrophotometer (UV-6000, Shanghai Yuanyi Apparatus Co., Ltd, China) in the wavelength of 280 nm. The calibration curve of BSA concentration was consistent with those in previous reports (Tong *et al.* 2020).

The tested membranes were rinsed repeatedly with deionized water. Subsequently, the pure water recovery ratios of the prepared UF membranes were calculated using Equation (5).

$$FRR(\%) = \frac{J_r}{J_w} \times 100\% \tag{5}$$

where FRR (%) is the pure water recovery ratio, and J_r and J_w are the original pure and recovered water fluxes ($L{\cdot}m^{-2}{\cdot}h^{-1}$) after the washing procedure, respectively.

2.5. Performance of membrane separation industrial papermaking wastewater

The industrial wastewater was obtained from reverse osmosis concentrated water from a paper mill in Suzhou. The wastewater is tested for pH, COD, turbidity, conductivity, and various anions and cations (Table 2).

The laboratory self-made cross-flow device was used for reverse osmosis (RO) concentrated water filtration experiments. PVDF UF membrane and PVDF-g-IBMA UF membrane were selected to test their performance. The pressure was set to 0.1 MPa. The effective area of the device is 2.83 cm^2.The experimental measurement time was set to 120 min.

3. RESULTS AND DISCUSSION

3.1. Characterization of PVDF-g-IBMA copolymer UF membrane

3.1.1. ^{1}H NMR

The structures of the PVDF homopolymer and PVDF-g-IBMA copolymer were verified using ^{1}H NMR spectroscopy (Figure 3 and Table 3). The peaks observed at 2.25 and 2.89 ppm in the ^{1}H NMR spectra of the copolymers corresponded to the $-CF_2CH_2CH_2CF_2-$ (head-to-head, hh) and $-CH_2CF_2CH_2CF_2-$ (head-to-tail, ht) of PVDF, respectively. In addition, the

Table 2 | RO concentrated water quality monitoring

Parameter	Unit	Value	Parameter	Unit	Value
COD	mg/L	720	Cu^{2+}	mg/L	79.7
Turbidity	NTU	1.68	K^+	mg/L	0
Conductivity	ms/cm	4.74	Ca^{2+}	mg/L	626.8
pH	/	7.20	Na^+	mg/L	1,367.0
SO_4^{2-}	mg/L	464.7	Fe^{2+}	mg/L	0.1
Cl^-	mg/L	973.2	Al^{3+}	mg/L	0
NO_3^-	mg/L	8.1	Mg^{2+}	mg/L	168.4

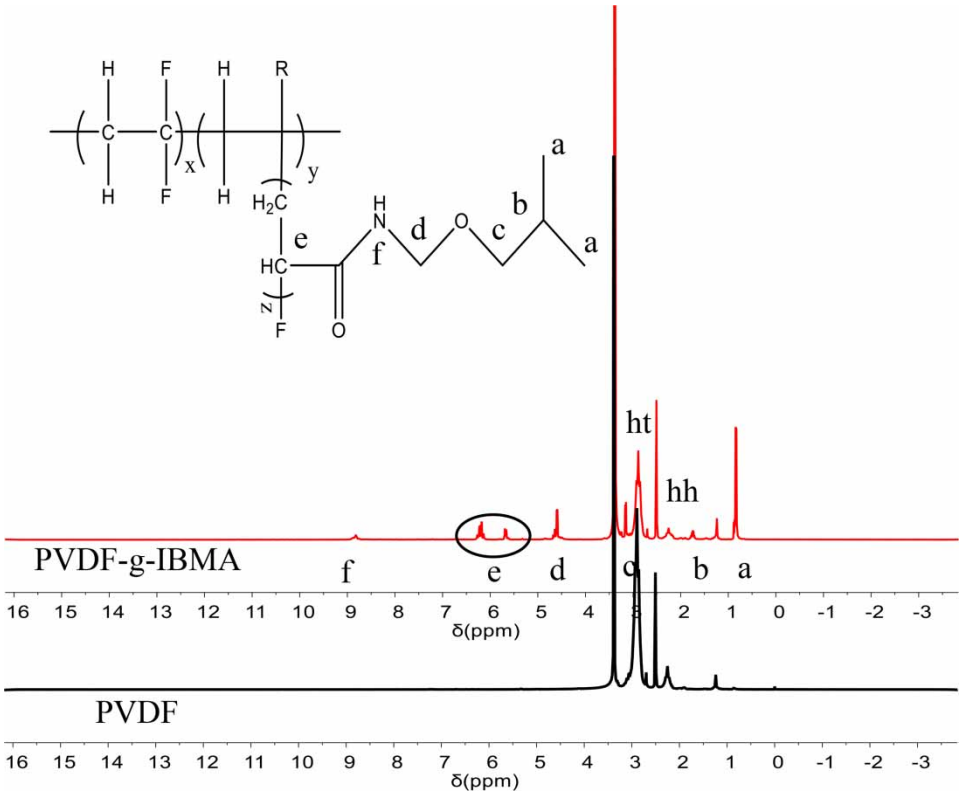

Figure 3 | The ^{1}H NMR spectra of the PVDF homopolymer and PVDF-g-IBMA copolymer.

Table 3 | The peak area of PVDF-g-IBMA copolymer in ^{1}H NMR spectra

I_x	I_a	I_b	I_c	I_d	I_e	I_f	I_{hh}	I_{ht}
	1.00	0.18	0.29	0.47	0.55	0.17	0.58	3.84

characteristic peaks of methyl, methane, and N–H were observed at $\delta = 0.91$ ppm (a), $\delta = 1.24$ ppm (b), and $\delta = 8.82$ ppm (f), respectively. The remaining peaks observed in the ^{1}H NMR spectra were the peaks of CH_2. Furthermore, extra resonances were inspected in the ^{1}H NMR spectrum of the PVDF-g-IBMA copolymer, which corresponded to the protons in IBMA, verifying the existence of IBMA in the PVDF-g-IBMA copolymers. In addition, the molar and mass fractions of IBMA were 7.43% and 16.47%, respectively.

3.1.2. FTIR spectroscopy

FTIR spectroscopy was carried out to verify the synthesis of PVDF-g-IMBA copolymer UF membrane. Several peaks were observed in the FTIR of the PVDF-g-IMBA UF membrane compared with that of the PVDF UF membrane (Figure 4). The peaks observed at 1,541 and 1,667 cm^{-1} could be ascribed to the bending vibrations of C–N–H and C = O, respectively, whereas those at 2,830–2,940 cm^{-1} could be assigned to the stretching vibrations of CH_2 and CH_3. These observations confirmed the successful synthesis of PVDF-g-IBMA copolymer.

3.1.3. DSC analysis

The melting point of the PVDF-g-IBMA copolymer was analyzed using DSC analysis. The melting point of the PVDF-g-IBMA copolymer was 174.2 °C, which was higher than that of the PVDF homopolymer (170.2 °C) (Figure 5). The increase in the melting point of PVDF corresponded to the change in the crystal form of the PVDF-g-IBMA copolymer. Thermogravimetric analysis further confirmed the successful grafting of IBMA onto PVDF.

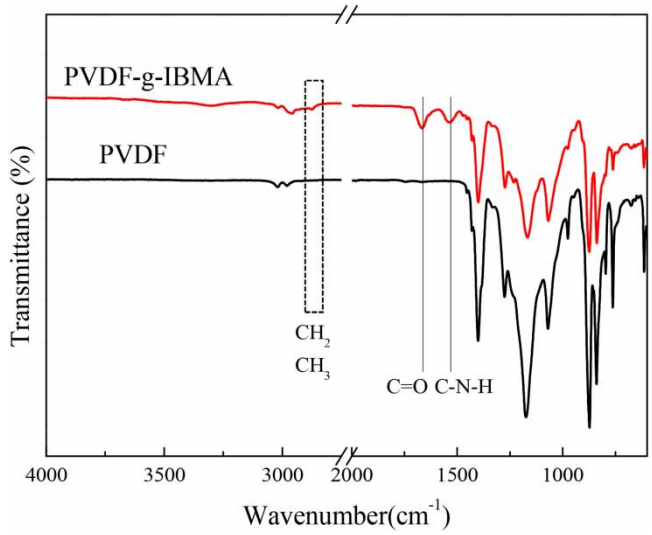

Figure 4 | FT-IR/ATR spectra of PVDF homopolymer and PVDF-g-IBMA copolymer UF membrane.

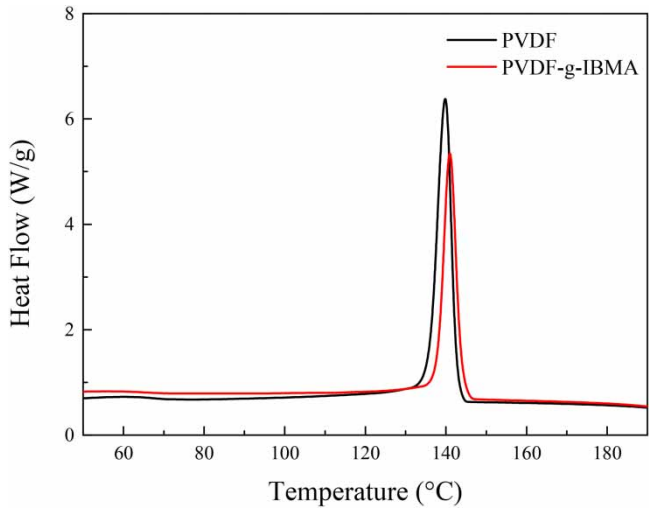

Figure 5 | DSC analysis of PVDF homopolymer and PVDF-g-IBMA copolymer UF membrane.

3.1.4. Casting solution viscosity

As shown in Figure 6, the viscosity of PVDF-g-IBMA UF casting membrane solution increased with an increase in the amount of the PVDF-g-IBMA copolymer in the casting solution, in the order of I15 < I20 < I25. In addition, the viscosity of PVDF-g-IBMA copolymer casting solution was higher than that of pure PVDF homopolymer casting solution with the same polymer concentration. An increase in the viscosity of the membrane casting solution hindered the exchange of the solvent and non-solvent during UF membrane formation and affected phase separation. However, the PVDF-g-IBMA copolymer contained a hydrophilic amide group (–NHCO–) that increased the phase rate of its membrane formation. These results indicated that the viscosity and hydrophilic chains of the casting solution affected the phase conversion rate during membrane formation, thus affecting the structure and performance of the prepared membrane owing to the competition between the two factors.

3.1.5. Membrane hydrophilicity

To illustrate the surface wettability of the PVDF-g-IBMA copolymer UF membrane, the DWCAs of the PVDF-g-IBMA UF membranes were measured and compared with those of the pure PVDF UF membranes (Figure 7). Within 180 s, the CA of the PVDF-g-IBMA copolymer membrane surface decreased. This was because penetration is a dynamic process, and

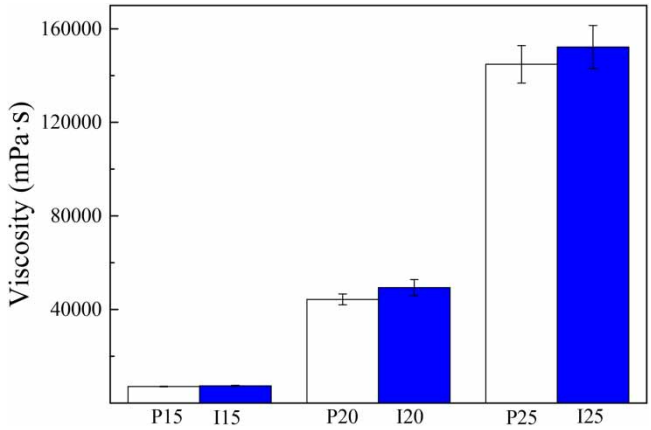

Figure 6 | Casting solution viscosity of the PVDF homopolymer and PVDF-g-IBMA copolymer casting solution.

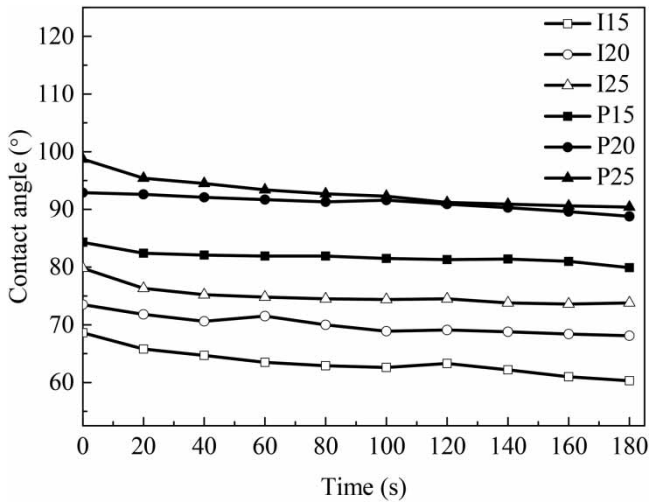

Figure 7 | DCA of the PVDF homopolymer and PVDF-g-IBMA copolymer UF membrane.

the CA of the membrane surface changed over time. In addition, the initial CAs of the pure PVDF UF membranes were larger than those of the PVDF-g-IBMA UF membrane. After 180 s, the stable CAs of I15, I20, and I25 were 60.3°, 68.1°, and 73.8°, respectively, which were less than those of the pure PVDF UF membranes. This indicated that the PVDF-g-IBMA UF membranes exhibited better hydrophilic performance than the PVDF membranes. Moreover, the surface of the PVDF-g-IBMA UF membrane was rich in IBMA hydrophilic chains. The hydrophilic amide groups in IBMA formed hydrogen bonds with H_2O molecules and formed a water layer, which isolated pollutants. The addition of hydrophilic groups changes the hydrophilic properties of the membrane. However, as the concentration of hydrophilic substances increases, the migration resistance became larger. As a result, there are more hydrophilic groups on the surface of the membrane at lower concentration, which leads to the decrease of the contact angle.

3.1.6. SEM analysis

As shown in Figure 8, the surface and cross-sectional morphologies images of the PVDF-g-IBMA copolymer UF membranes were investigated using SEM. The surface morphology characteristics of the PVDF-g-IBMA UF membranes were similar to those of the pure PVDF UF membranes (Tong *et al.* 2020). As the concentration of the membrane casting solution increased, the number of pores on the surface of the formed UF membrane decreased. Consequently, the surface of I15 had the most abundant pores. In addition, notable pore structures and sponge layers were observed in the cross-sectional morphology

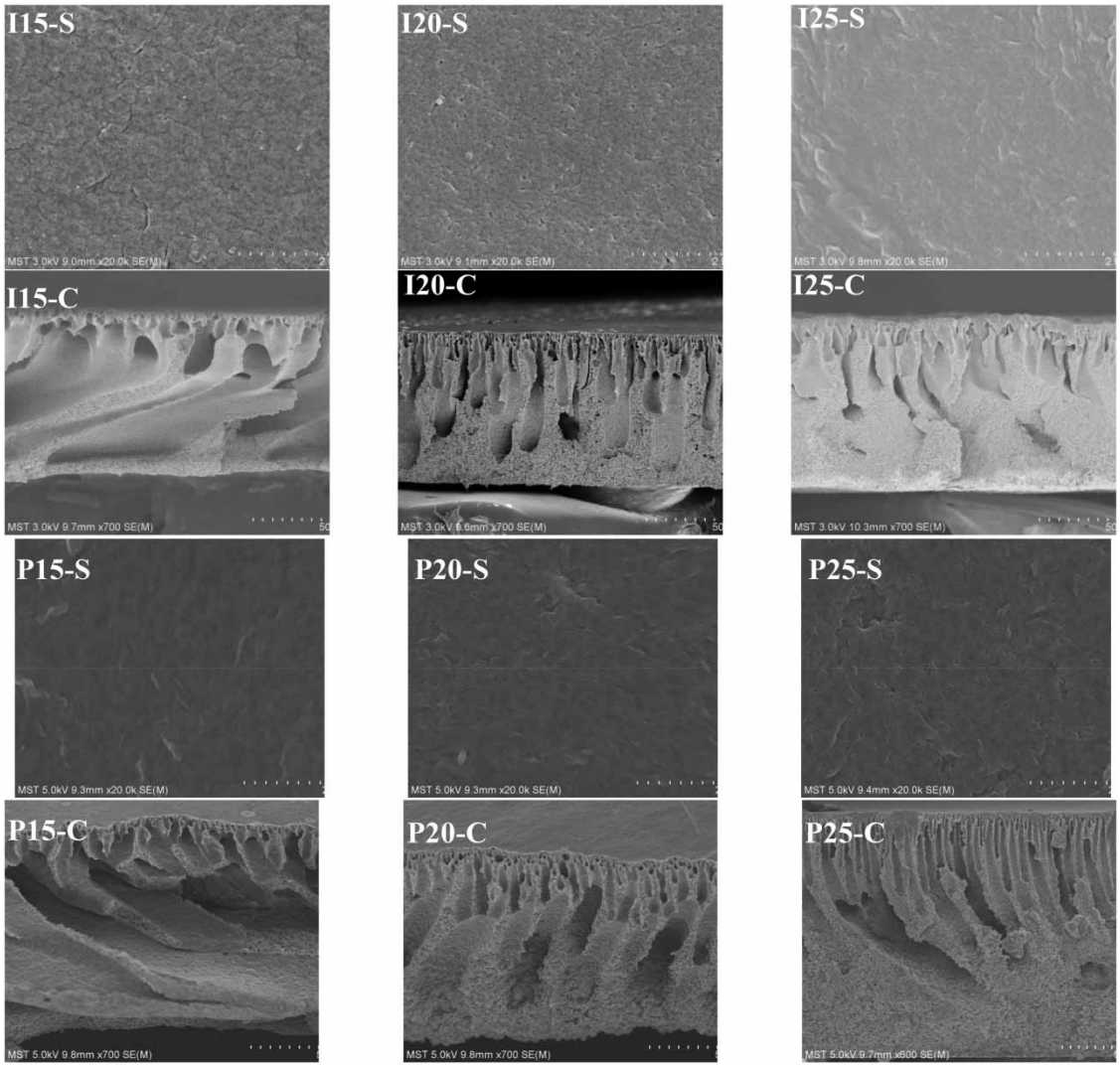

Figure 8 | SEM images of the surface and cross-section morphologies of the PVDF-g-IBMA copolymer UF membrane and the PVDF homopolymer.

of the PVDF-g-IBMA UF membranes. Because the casting solution of I15 had the lowest viscosity, it exhibited the highest phase inversion rate during phase inversion, which resulted in the formation of notable finger-like macroporous structures. As the concentration of casting solution increased, the number of finger-like pores gradually decreased, and the area of the sponge layer gradually increased. Moreover, the SEM image revealed the successful formation of membranes with finger-like macropores due to the rapid exchange rate of the solvent and non-solvent.

3.1.7. EDX analysis

The distribution of elements in the cross-section of the PVDF-g-IBMA copolymer UF membrane is shown in Figure 9. After scanning the cross-sectional energy spectrum, in addition to the carbon and fluorine atoms of PVDF, the oxygen and nitrogen atoms of IBMA were observed, confirming the successful synthesis of the PVDF-g-IBMA copolymer. Notable pore structures and sponge layers were observed at the upper and lower parts of the cross-section, respectively. However, the distribution ratio of nitrogen atoms in the upper and lower parts of the cross-section was 1:1, indicating that the hydrophilic chains of IBMA migrated to surface of pores (Oikonomoua *et al.* 2017).

3.1.8. AFM analysis

The AFM images of the membrane surface on a scanning area of 5 μm by 5 μm are shown in Figure 10. The average roughness of the PVDF-g-IBMA membrane is much lower than that of the PVDF membrane (P15 = 147 nm, P20 = 267 nm,

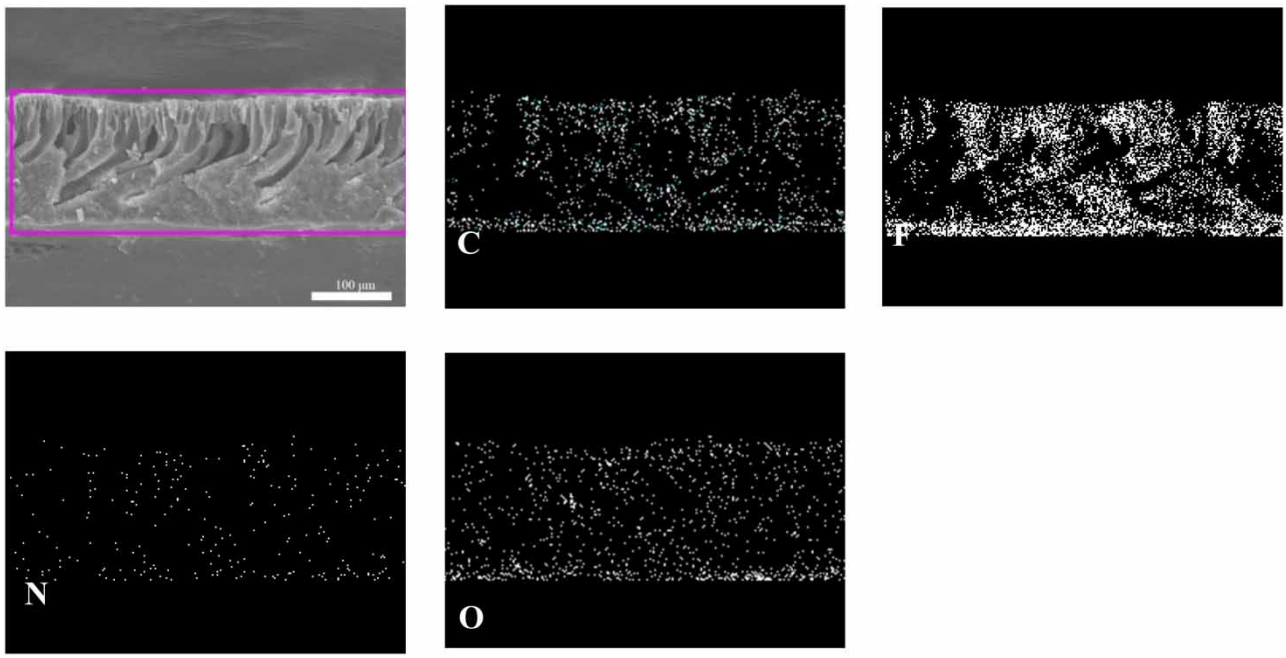

Figure 9 | EDX mapping of the PVDF-g-IBMA copolymer UF membrane.

P25 = 129 nm) (Tong *et al.* 2020). The surface roughness of I20 is 39.8 nm, while it is 147 nm for P15. Therefore, the PVDF-g-IBMA membrane with a smoother surface may have greater antifouling ability.

3.1.9. Mechanical properties

In order to investigate the mechanical properties of PVDF and PVDF-g-IBMA membrane, the tensile strength and elongation at break values were tested. As listed in Table 4, compared with the PVDF membrane, the tensile strength and elongation at break of PVDF-g-IBMA membrane were reduced. It indicated that the mechanical properties of the PVDF-g-IBMA membrane reduced a little.

3.2. Membrane performance

3.2.1. Pure water flux and MWCO

The pure water fluxes of the PVDF and PVDF-g-IBMA copolymer UF membranes are shown in Figure 11. As the concentration of casting solution increased, the pure water fluxes of the UF membranes decreased. The pure water fluxes of the PVDF-g-IBMA UF membranes were significantly higher than those of the pure PVDF UF membranes. The pure water flux of I15 was 432.8 $L{\cdot}m^{-2}{\cdot}h^{-1}$, which was higher than those of the other PVDF-g-IBMA UF membranes and 7.5 times higher than that of P15. The pure water fluxes of I20 and I25 were 7.4 and 23.8 times higher than those of P20 and P25, respectively. These results indicated that the PVDF-g-IBMA membranes had denser pores than the pure PVDF UF membranes, and the migration effect of hydrophilic chains to the surface of the PVDF-g-IBMA UF membranes was more notable.

The MWCO values of I15, I20, and I25 were 43.7, 23.2, and 16.6 kDa, respectively. The MWCO values of the PVDF-g-IBMA UF membranes were higher than those of the pure PVDF UF membranes of the same concentration. These results were consistent with the microporous structure and higher pure water fluxes of the PVDF-g-IBMA UF membranes.

3.2.2. Anti-fouling performance of the PVDF-g-IBMA copolymer UF membrane

The BSA rejection and flux recovery rates of the PVDF-g-IBMA copolymer UF membranes are listed in Table 5. The BSA rejection rates of the PVDF-g-IBMA UF membranes were higher than those of the PVDF UF membranes. The BSA rejection rate of I15 (88.4%) was higher than that of P15 (85.7%). As the concentration of the casting solution for the PVDF-g-IBMA membranes increased, the BSA rejection rate of the copolymer UF membranes increased. Consequently, I25 had the highest BSA rejection rate (92.7%). Furthermore, the pure water flux recovery rates of the PVDF-g-IBMA UF membranes were higher

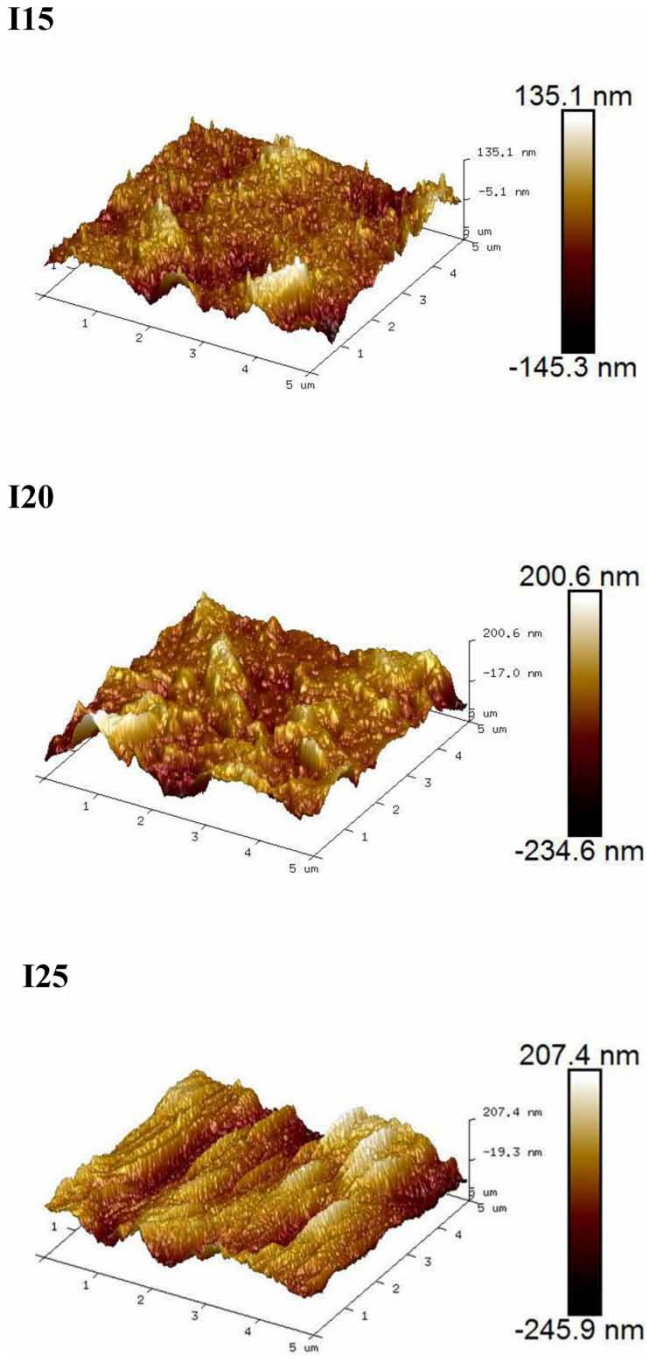

Figure 10 | 3D AFM images of the PVDF and PVDF-g-IBMA membrane surfaces.

than those of the pure PVDF UF membranes. The pure water flux recovery rate of I25 was 89.5%, which was significantly higher than that of the pure PVDF UF membrane (P20, 78.0%).

As the concentration of the copolymer casting solution increased, the BSA initial and stable fluxes of the PVDF-g-IBMA UF membranes decreased (Figure 12). The stable fluxes of the PVDF-g-IBMA UF membranes were higher than those of the pure PVDF UF membranes. The stable flux of I15 (164.6 $L \cdot m^{-2} \cdot h^{-1}$) was significantly higher than that of P15 (27.8 $L \cdot m^{-2} \cdot h^{-1}$). The stable fluxes of I20 and 125 were significantly higher than those of P20 and P25. These results corresponded to the improved antifouling of the PVDF-g-IBMA UF membranes compared with those of the PVDF membranes (Tong *et al.* 2020).

Table 4 | Mechanical properties of PVDF and PVDF-g-IBMA membrane

	Elongation at break values (%)	Tensile strength (MPa)
P15	18.31	1.94
P20	20.04	2.42
P25	32.31	3.74
I15	15.30	1.44
I20	18.75	1.90
I25	26.11	3.13

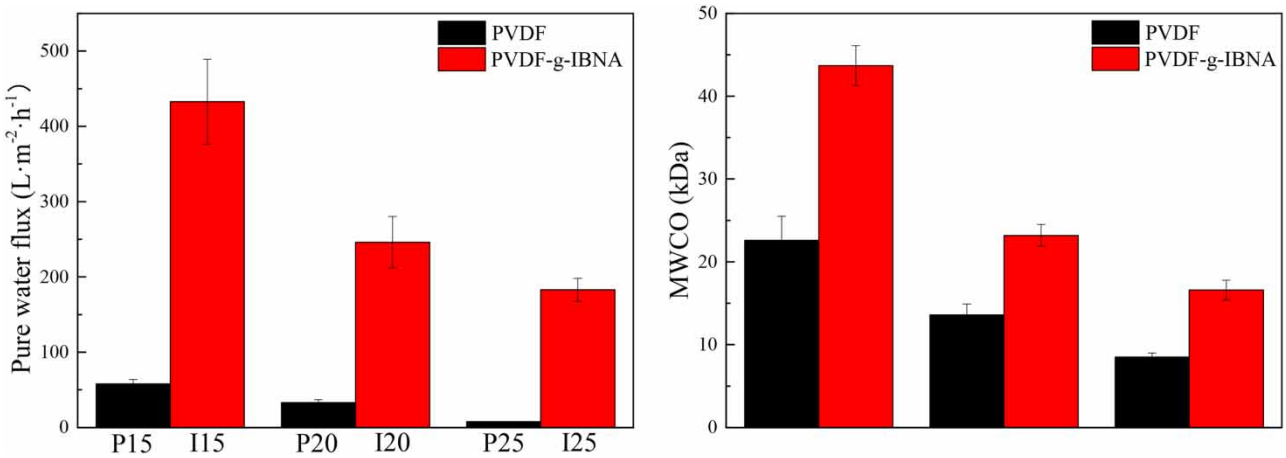

Figure 11 | Pure water flux and MWCO of the PVDF-g-IBMA copolymer UF membrane.

Table 5 | BSA rejection and FRR of the PVDF-g-IBMA copolymer UF membrane

Membrane code	BSA rejection(%)	FRR(%)
I15	88.4 ± 2.7	90.8 ± 3.1
I20	90.5 ± 3.8	92.3 ± 2.6
I25	92.7 ± 1.6	89.5 ± 2.5
P15 (Tong *et al.* 2020)	85.7 ± 3.4	79.0 ± 2.1
P20 (Tong *et al.* 2020)	86.4 ± 2.2	82.9 ± 2.4
P25 (Tong *et al.* 2020)	88.9 ± 2.6	78.0 ± 3.6

Compared with published modified PVDF membranes, including PVDF-g-NMA, PVDF-g-PEGMA, PVDF-g-POEM, PVDF-g-PMABS, PVDF-g-(PAMCO-PAA), The pure water flux of I15 (432.8 $L{\cdot}m^{-2}{\cdot}h^{-1}$) was significantly higher than those of the previously modified copolymer membranes (Table 6).

3.3. Treatment of RO-concentrated water using the PVDF-g-IBMA copolymer ultrafiltration membrane

The performances of the pure PVDF and PVDF-g-IBMA UF membranes for the treatment of RO-concentrated water are shown in Table 7 and Figure 13. The COD and turbidity removal rates of the PVDF-g-IBMA UF membranes were significantly improved compared with those of the pure PVDF UF membranes. Under the same casting solution concentration, the actual wastewater treatment effect of the PVDF-g-IBMA copolymer UF membranes was stronger than those of the PVDF UF membranes. The COD and turbidity removal rates of I25 were 61.5% and 92.8%, respectively, which were higher than those of the

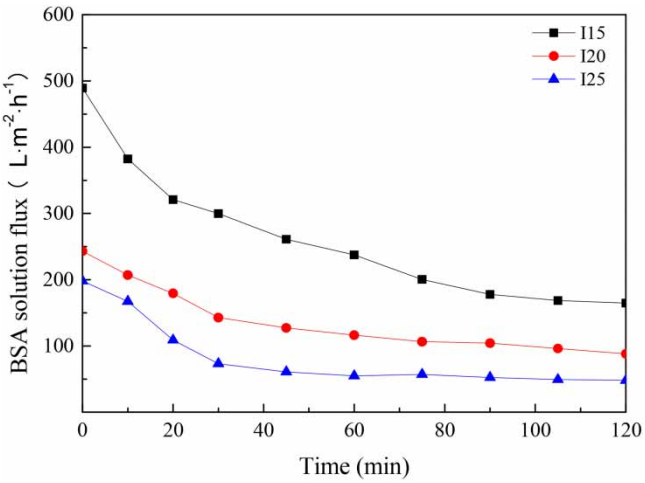

Figure 12 | Time-dependent BSA solution flux of the PVDF-g-IBMA copolymer UF membrane.

Table 6 | Comparison with the results of literatures

Membrane	Operating conditions	Pure water ($L \cdot m^{-2} \cdot h^{-1}$)	Rejection (%)	References
PVDF-g-NMA	0.1 MPa, 1.0 $g \cdot L^{-1}$BSA	272	93.7	Tong *et al.* (2020)
PVDF-g-PMABS	0.1 MPa, 1.0 $g \cdot L^{-1}$BSA	136	98.6	Chen *et al.* (2018)
PVDF-g-(PAMCO-PAA)	0.1 MPa, 1.0 $g \cdot L^{-1}$BSA	130	96.3	Xu *et al.* (2017)
PVDF-g-PEGMA	0.1 MPa, 1.0 wt.% BSA	116	66.3	Hashim *et al.* (2009)
PVDF-g-POEM	0.1 MPa, 1.0 $g \cdot L^{-1}$BSA	130	83.5	Moghareh Abed *et al.* (2013)
This work	0.1 MPa, 1.0 $g \cdot L^{-1}$BSA	432	88.4	

Table 7 | Water quality of liquid penetration after filtering RO concentrated water with PVDF-g-IBMA copolymer UF membrane

Membrane	Permeate side COD (mg/L)	COD removal rate (%)	Permeate turbidity (NTU)	Turbidity removal rate (%)
P15	600	16.7	0.176	89.5
P20	510	29.2	0.161	90.4
P25	470	34.7	0.159	90.5
I15	419	41.8	0.165	90.2
I20	365	49.3	0.140	91.7
I25	277	61.5	0.121	92.8

other samples. The RO concentrated water flux of the membranes decreased over time. The hydrophilicity of the PVDF-g-IBMA copolymer UF membranes was better than that of the PVDF UF membranes. Consequently, the initial and stable fluxes of the PVDF-g-IBMA copolymer UF membranes were significantly higher than those of the PVDF UF membranes.

4. CONCLUSION

A novel PVDF-g-IBMA amphiphilic copolymer was successfully synthesized via ultraviolet-induced Cu(II)-mediated RDRP and used to fabricate a UF membrane using the NIPS method. ^{1}H NMR, FTIR spectroscopy, and DSC analysis confirmed the successful synthesis of the PVDF-g-IBMA copolymer. The hydrophilicity and antifouling performance of the prepared PVDF-g-IBMA copolymer UF membranes were improved compared with those of the pure PVDF UF membranes. The contact angle of the UF membrane reduced to 60.3° after 180 s, and the pure water flux of the UF membrane was

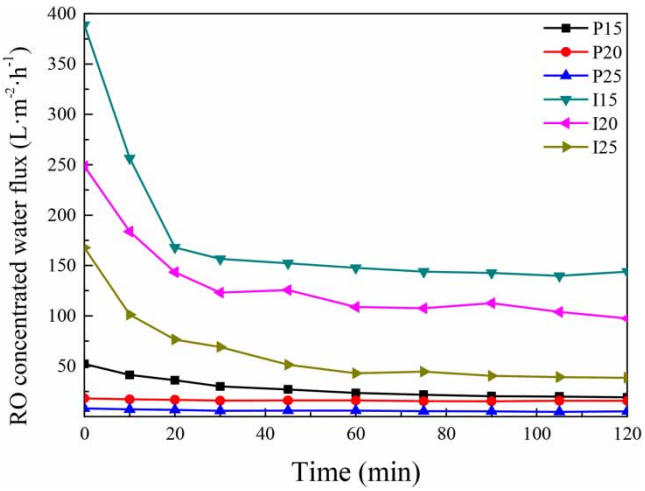

Figure 13 | Time-dependent RO concentrated water fluxes of PVDF homopolymer UF membrane and PVDF-g-IBMA copolymer UF membrane.

432.8 $L{\cdot}m^{-2}{\cdot}h^{-1}$, which was 7.5 times higher than that of the pure PVDF UF membrane. The MWCO, BSA rejection rate, and pure water flux of the UF membrane were 43.7 kDa, 88.4%, and 90.8%, respectively. The stable flux of the PVDF-g-IBMA UF membrane for filtrating BSA solution was 164.6 $L{\cdot}m^{-2}{\cdot}h^{-1}$, which was higher than that of the pure PVDF UF membrane (27.8 $L{\cdot}m^{-2}{\cdot}h^{-1}$).

For the treatment of papermaking wastewater, the COD was reduced from 720 to 277 mg/L with a removal rate of 61.5%. The turbidity decreased from 1.68 to 0.12 NTU with a removal rate of 92.8%. And the initial and stable fluxes of the PVDF-g-IBMA copolymer UF membranes were significantly higher than those of the pure PVDF UF membranes, indicating the potential of prepared membrane for treating papermaking wastewater.

ACKNOWLEDGEMENTS

This work was supported by Tianjin Synthetic Biotechnology Innovation Capacity Improvement Project (TSBICIP-KJGG-003), Qinglan Plan of Jiangsu Education Department and the National Key R&D Program of China (2017YFD0400402).

DECLARATION OF COMPETING INTERESTS

The authors declare that they have no known competing financial interests or personal relationships that could have appeared to influence the work reported in this paper.

CREDIT AUTHORSHIP CONTRIBUTION STATEMENT

Yujia Tong: Conceptualization, Methodology, Software, Formal analysis, Investigation, Writing – Original Draft, Writing – Review and Editing. **Wenlong Ding:** Validation, Investigation. **Lijian Shi:** Validation, Investigation. **Weixing Li:** Writing – Review and Editing, Supervision, Funding acquisition.

DATA AVAILABILITY STATEMENT

All relevant data are included in the paper or its Supplementary Information.

REFERENCES

Chen, F., Shi, X., Chen, X. & Chen, W. 2018 Preparation and characterization of amphiphilic copolymer PVDF-g-PMABS and its application in improving hydrophilicity and protein fouling resistance of PVDF membrane. *Applied Surface Science* **427**, 787–797.

Chen, M., Ding, W., Zhou, M., Zhang, H., Ge, C., Cui, Z. & Xing, W. 2021 Fouling mechanism of PVDF ultrafiltration membrane for secondary effluent treatment from paper mills. *Chemical Engineering Research and Design* **167**, 37–45.

Chuang, Y.-M., Ethirajan, A. & Junkers, T. 2014 Photoinduced sequence-controlled copper-mediated polymerization: synthesis of decablock copolymers. *ACS Macro Letters* **3** (8), 732–737.

Cui, Z., Tang, X., Li, W., Liu, H., Zhang, J., Wang, H. & Li, J. 2019 EVOH in situ fibrillation and its effect of strengthening, toughening and hydrophilic modification on PVDF hollow fiber microfiltration membrane via TIPS process. *Journal of Materials Science* **54** (7), 5971–5987.

Gao, W., Liang, H., Ma, J., Han, M., Chen, Z.-l., Han, Z.-s. & Li, G.-b. 2011 Membrane fouling control in ultrafiltration technology for drinking water production: a review. *Desalination* **272** (1–3), 1–8.

Gao, Y., Qin, J., Wang, Z. & Østerhus, S. W. 2019 Backpulsing technology applied in MF and UF processes for membrane fouling mitigation: a review. *Journal of Membrane Science* **587**, 117136.

Gönder, Z. B., Arayici, S. & Barlas, H. 2012 Treatment of pulp and paper mill wastewater using utrafiltration process: optimization of the fouling and rejections. *Industrial & Engineering Chemistry Research* **51** (17), 6184–6195.

Guillen, G. R., Pan, Y., Li, M. & Hoek, E. M. V. 2011 Preparation and characterization of membranes formed by nonsolvent induced phase separation: a review. *Industrial & Engineering Chemistry Research* **50** (7), 3798–3817.

Haq, I., Mazumder, P. & Kalamdhad, A. S. 2020 Recent advances in removal of lignin from paper industry wastewater and its industrial applications – a review. *Bioresour Technol* **312**, 123636.

Hashim, N. A., Liu, F. & Li, K. 2009 A simplified method for preparation of hydrophilic PVDF membranes from an amphiphilic graft copolymer. *Journal of Membrane Science* **345**, 134–141.

Hu, X., Cui, G., Zhang, Y., Zhu, N. & Guo, K. 2018a Copper(II) photoinduced graft modification of P(VDF- co -CTFE). *European Polymer Journal* **100**, 228–232.

Hu, X., Cui, G., Zhu, N., Zhai, J. & Guo, K. 2018b Photoinduced Cu(II)-Mediated RDRP to P(VDF-co-CTFE)-g-PAN. *Polymers (Basel)* **10** (1), 68.

Lei, H., Liu, L., Huang, L., Li, W. & Xing, W. 2018 Novel anti-fouling PVDF-g-THweFMA copolymer membrane fabricated via photoinduced Cu(II)-mediated reversible deactivation radical polymerization. *Polymer* **157**, 1–8.

Li, R., Li, J., Rao, L., Lin, H., Shen, L., Xu, Y., Chen, J. & Liao, B.-Q. 2021 Inkjet printing of dopamine followed by UV light irradiation to modify mussel-inspired PVDF membrane for efficient oil-water separation. *Journal of Membrane Science* **619**, 118790.

Liu, F., Hashim, N. A., Liu, Y., Abed, M. R. M. & Li, K. 2011 Progress in the production and modification of PVDF membranes. *Journal of Membrane Science* **375** (1–2), 1–27.

Matyjaszewski, K. 2020 Amphiphilic polymer co-networks: synthesis, properties, modelling and applications. Edited by Costas S. Patrickios. *Angewandte Chemie International Edition* **60** (3), 1064–1064.

Minehara, H., Dan, K., Ito, Y., Takabatake, H. & Henmi, M. 2014 Quantitative evaluation of fouling resistance of PVDF/PMMA-g-PEO polymer blend membranes for membrane bioreactor. *Journal of Membrane Science* **466**, 211–219.

Moghareh Abed, M. R., Kumbharkar, S. C., Groth, A. M. & Li, K. 2013 Economical production of PVDF-g-POEM for use as a blend in preparation of PVDF based hydrophilic hollow fibre membranes. *Separation and Purification Technology* **106**, 47–55.

Oikonomoua, E., Karpati, S., Gassara, S., Deratani, A., Beaume, F., Lorain, O., Tencé-Girault, S. & Norvez, S. 2017 Localization of antifouling surface additives in the pore structure of hollow fiber PVDF membranes. *Journal of Membrane Science* **538**, 77–85.

Park, S.-H., Ahn, Y., Jang, M., Kim, H.-J., Cho, K. Y., Hwang, S. S., Lee, J.-H. & Baek, K.-Y. 2018 Effects of methacrylate based amphiphilic block copolymer additives on ultra filtration PVDF membrane formation. *Separation and Purification Technology* **202**, 34–44.

Shen, Z., Cai, N., Xue, Y., Yu, B., Wang, J., Song, H., Deng, H. & Yu, F. 2020 Porous SBA-15/cellulose membrane with prolonged anti-microbial drug release characteristics for potential wound dressing application. *Cellulose* **27** (5), 2737–2756.

Sierke, J. & Ellis, A. V. 2019 Cross-linking of dehydrofluorinated PVDF membranes with thiol modified polyhedral oligomeric silsesquioxane (POSS) and pure water flux analysis. *Journal of Membrane Science* **581**, 362–372.

Sri Abirami Saraswathi, M. S., Rana, D., Divya, K., Alwarappan, S. & Nagendran, A. 2018 Fabrication of anti-fouling PVDF nanocomposite membranes using manganese dioxide nanospheres with tailored morphology, hydrophilicity and permeation. *New Journal of Chemistry* **42** (19), 15803–15810.

Sun, C.-C., Zhou, M.-Y., Yuan, J.-J., Yan, Y., Song, Y.-Z., Fang, L.-F. & Zhu, B.-K. 2020 Membranes with negatively-charged nanochannels fabricated from aqueous sulfonated polysulfone nanoparticles for enhancing the rejection of divalent anions. *Journal of Membrane Science* **602**, 117692.

Toczyłowska-Mamińska, R. 2017 Limits and perspectives of pulp and paper industry wastewater treatment – A review. *Renewable and Sustainable Energy Reviews* **78**, 764–772.

Tong, Y., Huang, L., Zuo, C., Li, W. & Xing, W. 2020 Novel PVDF-g-NMA copolymer for fabricating the hydrophilic ultrafiltration membrane with good antifouling property. *Industrial & Engineering Chemistry Research* **60** (1), 541–550.

Wu, Q., Tiraferri, A., Wu, H., Xie, W. & Liu, B. 2019 Improving the performance of PVDF/PVDF-g-PEGMA ultrafiltration membranes by partial solvent substitution with Green solvent dimethyl sulfoxide during fabrication. *ACS Omega* **4** (22), 19799–19807.

Xu, R., Feng, Q., He, Y., Yan, F., Chen, L. & Zhao, Y. 2017 Dual functionalized poly(vinylidene fluoride) membrane with acryloylmorpholine and argatroban to improve antifouling and hemocompatibility. *Journal of Biomedical Materials Research Part A* **105** (1), 178–188.

Zhang, X. & Dai, Y. 2019 Recent development of brush polymers via polymerization of poly(ethylene glycol)-based macromonomers. *Polymer Chemistry* **10** (18), 2212–2222.

Zhang, B., Yu, S., Zhu, Y., Shen, Y., Gao, X., Shi, W. & Hwa Tay, J. 2020 Adsorption mechanisms of crude oil onto polytetrafluoroethylene membrane: kinetics and isotherm, and strategies for adsorption fouling control. *Separation and Purification Technology* **235**, 116212.

Zhao, J., Han, H., Wang, Q., Yan, C., Li, D., Yang, J., Feng, X., Yang, N., Zhao, Y. & Chen, L. 2019 Hydrophilic and anti-fouling PVDF blend ultrafiltration membranes using polyacryloylmorpholine-based triblock copolymers as amphiphilic modifiers. *Reactive and Functional Polymers* **139**, 92–101.

Zou, H., Ren, X. & Zhang, J. 2020 Fabrication of a Bi_2O_3 surface-modified polyvinylidene fluoride membrane via an ultraviolet photografting method: improving hydrophilicity and degree of acrylic acid grafting. *Industrial & Engineering Chemistry Research* **59** (14), 6580–6588.

First received 24 June 2021; accepted in revised form 26 August 2021. Available online 7 September 2021